INSTITUTE OF PHYSICS PUBLISHING SEMICONDUCTOR SCIENCE AND TECHNOLOGY

Semicond. Sci. Technol. **20** (2005) 1087–1095 doi:10.1088/0268-1242/20/10/018

Thermal resistance and optimal fill factor of a high power diode laser bar

B Laikhtman[1,3], A Gourevitch[2], D Westerfeld[2,3], D Donetsky[2] and G Belenky[2]

[1] Racah Institute of Physics, Hebrew University, Jerusalem 91904, Israel
[2] Department of Electrical Engineering, State University of New York at Stony Brook, Stony Brook, NY 11794, USA
[3] Power Photonic, 214 Old Chemistry, Stony Brook, NY 11794-3717, USA

Received 6 May 2005, in final form 25 August 2005
Published 19 September 2005
Online at stacks.iop.org/SST/20/1087

Abstract
Using analytical methods, we obtain compact theoretical expressions for the electrical and thermal resistances of a laser bar as a function of its fill factor. The theoretically determined values of the thermal resistance are in excellent agreement with the measured ones. We use the theoretical values of the electrical and thermal resistances to find the fill factor that gives the maximal output power for a given active region temperature and the fill factor that gives the minimal active region temperature for a given output power. The optimal fill factor is dependent on the bar operating regime; higher power operation favours the use of higher fill factors to minimize the active region temperature rise.

(Some figures in this article are in colour only in the electronic version)

1. Introduction

A growing demand for high power optical sources led to a race to improve device reliability and increase output power. Technological development produced a gradual increase of single laser output power; however, a significant improvement took place with the fabrication of laser bars. The laser bar contains numerous individual laser emitters arranged side-by-side to form a single monolithic array. A typical laser bar might contain twenty 100 μm wide emitters equally spaced to span a 1 cm wide bar. The fill factor for such an array is defined to be the ratio of pumped bar area to total bar area.

Two solutions are most evident for increasing the laser bar output power: one is to increase the current per emitter, and the other is to increase the number of emitters. Increasing the number of fixed-width emitters on a fixed-width bar is equivalent to reducing the distance between individual emitters (i.e. increasing the fill factor). Both solutions, however, encounter an overheating problem. An increased pumping current leads not only to an increased output power but also, due to limited efficiency, to an increased dissipated power. As a result, the temperature in the active region grows which reduces the carrier confinement and increases the rate of non-radiative recombination processes. This causes an efficiency reduction so that eventually the output power saturates with increased pumping current (thermal rollover) [1].

Reducing the distance between emitters operating at constant dissipated power results in a similar heating problem. Decreasing the separation between adjacent emitters in a laser bar causes mutual heating which also leads to an active region temperature rise and decreased efficiency [2]. A natural step is to reduce the distance between the emitters while also varying the pumping current in such a way that the total output power would increase. That is, we come to the problem of the optimal fill factor: finding the fill factor that allows for maximal laser bar output power.

Practically, however, laser bars are not normally operated in the regime of maximal output power. The laser temperature in this regime is quite high which reduces the device lifetime. The reliability issue leads to other approaches to the optimization problem: optimization of the distance between emitters to produce (1) maximal output power for a given active region temperature rise or (2) minimal active region temperature rise for a given output power.

Basically, all these approaches are related to the general problem of the optimization of the laser bar design. The search for the optimal fill factor when all other elements of the laser geometry (e.g., the width of the contact stripes) are fixed is an approach that allows an exact mathematical solution.

The calculation of the optimal fill factor is based on the standard phenomenological equations that describe the operation of a laser bar [1, 3]. Some of the main parameters in these equations, namely, the thermal resistance characterizing the cooling rate and the series resistance characterizing the power dissipated away from the active region, depend on the fill factor. The dependence is controlled by the laser design. To the best of our knowledge, no compact analytical expressions for the resistances have been suggested so far and this impedes the improvement of the temperature characteristics of laser bars. In this paper, we derive analytical expressions for the thermal and electrical series resistance for typical laser bar designs, and then use these expressions to find the optimal fill factor for a given laser bar architecture.

The central point in the evaluation of the electric resistance is the current spread calculation. In some previous publications, the current density was calculated under the assumption of constant density at the contact stripe which then falls off as the square of the distance away from the contact [4–8]. An exact analytical solution to the Laplace equation that controls the current spread when carrier diffusion can be neglected was obtained by Lengyel *et al* [9]. They studied a narrow stripe geometry where the width of the stripe is of the order of its distance from the active region. Similar models have been considered by Wilt [10], Joyce [11] and Agrawal [12]. A comprehensive comparison of these models has been made by Papannareddy *et al* [13]. The geometry considered by Lengyel *et al* [9] corresponded to the situation in ridge lasers. In high power lasers the width of the stripe is much larger than the cladding thickness, and the n-layer thickness is comparable to the stripe width. Previously, we have shown that such a relation leads to a high current density near the edges of the active region [14]. In this paper, we consider the current spread from a system of parallel stripes in a laser bar.

The thermal resistance substantially depends on the thermal conductivity and geometry of the heat spreader located between the laser and the heat sink [15, 16]. Determining the thermal resistance requires the solution of the thermal conductance equation with non-trivial boundary conditions. For this purpose, a finite element method is typically used [17, 18]. In the present paper, we use analytical approaches that allow one to understand the qualitative dependence of device characteristics on different parameters without performing the time consuming numerical calculation required in finite element methods.

The calculated electrical series resistance is weakly dependent on fill factor. In contrast, the dependence of the thermal resistance on the fill factor is substantial. The expression obtained for the thermal resistance gives an excellent agreement with measured values without any adjustable parameters [19]. Analytical results for both resistances facilitate the calculation of the optimal fill factor.

This paper is organized as follows. In section 2 we formulate the fill factor optimization problem for a laser bar. In sections 3 and 4, we present analytical solutions to the electrical and thermal problems and calculate the electric and thermal resistances. In section 5, we compare the theoretical and experimental values of the thermal resistance and present the theoretical results of the bar optimization.

2. Optimal fill factor

We consider a laser bar with N contact stripes with a distance a_1 between their centres (figure 1(*a*)). The laser bar is mounted on a heat spreader which conducts heat from the laser bar to the heat sink. The heat sink is assumed ideal, i.e., its temperature is fixed and does not depend on the power dissipated in the bar. We assume that the cooling conditions for all lasers in the bar are the same and we can neglect the edge effects. In other words, the difference between the cooling of the lasers close to the ends of the bar and those in the middle can be neglected and the temperature of their active regions is the same. Indeed, we did not detect any temperature difference between different lasers in a 25 W 1.47 μm laser array that contained 20 elements [19] (compare with [2]).

If $j_{\rm th}$ is the threshold current in one emitter and $j > j_{\rm th}$ is the pumping current then the optical power generated in this emitter is

$$p_{\rm opt} = \eta(j - j_{\rm th}) \tag{2.1}$$

where η is the differential efficiency. Well above the threshold the voltage drop across the active region, U_0, does not depend on the current and the power dissipated in one laser is

$$p_{\rm d} = U_0 j + rj^2 - p_{\rm opt}, \tag{2.2}$$

where r is the series resistance of one laser.

To make the result more general and avoid specifying the number of emitters (N) in a bar and the length of the bar it is convenient to deal with power dissipated per unit length of the bar, $Np_{\rm d}/L_{\rm b}$, where $L_{\rm b}$ is the length of the bar. The temperature of the active region is connected to the power dissipated per unit length by the relation $T = R_{\rm T}(Np_{\rm d}/L_{\rm b})$, where $R_{\rm T}$ is the thermal resistance of the unit length of the bar. At this stage it is convenient to introduce the fill factor that is defined as

$$f = \frac{Na}{L_{\rm b}} \tag{2.3}$$

where a is the width of the stripe. Then with the help of equations (2.1) and (2.2) the active region temperature can be expressed as

$$T = \frac{fR_{\rm T}}{a}[\eta j_{\rm th} + (U_0 - \eta)j + rj^2]. \tag{2.4}$$

The optical power per unit length of the bar, $P_{\rm opt} = Np_{\rm opt}/L_{\rm b}$, with the help of equation (2.1) can be written as

$$P_{\rm opt} = \frac{f\eta}{a}(j - j_{\rm th}). \tag{2.5}$$

The definition of $P_{\rm opt}$ and T by equations (2.4) and (2.5) is not complete for two reasons. The first is that $j_{\rm th}$ and η depend on T. With a good accuracy this dependence is usually described as

$$j_{\rm th} = j_{\rm r}\,{\rm e}^{(T-T_{\rm r})/T_0}, \tag{2.6a}$$

$$\eta = \eta_{\rm r}\,{\rm e}^{-(T-T_{\rm r})/T_1}, \tag{2.6b}$$

where $T_{\rm r}$ is the reference temperature and the constants $j_{\rm r}$, $\eta_{\rm r}$, T_0 and T_1 depend on the details of the laser structure.

The second reason is more serious and presents the main technical difficulty for the calculation of the optimal fill factor. Namely, both the thermal resistance and the series resistance depend on the fill factor. This dependence is controlled by

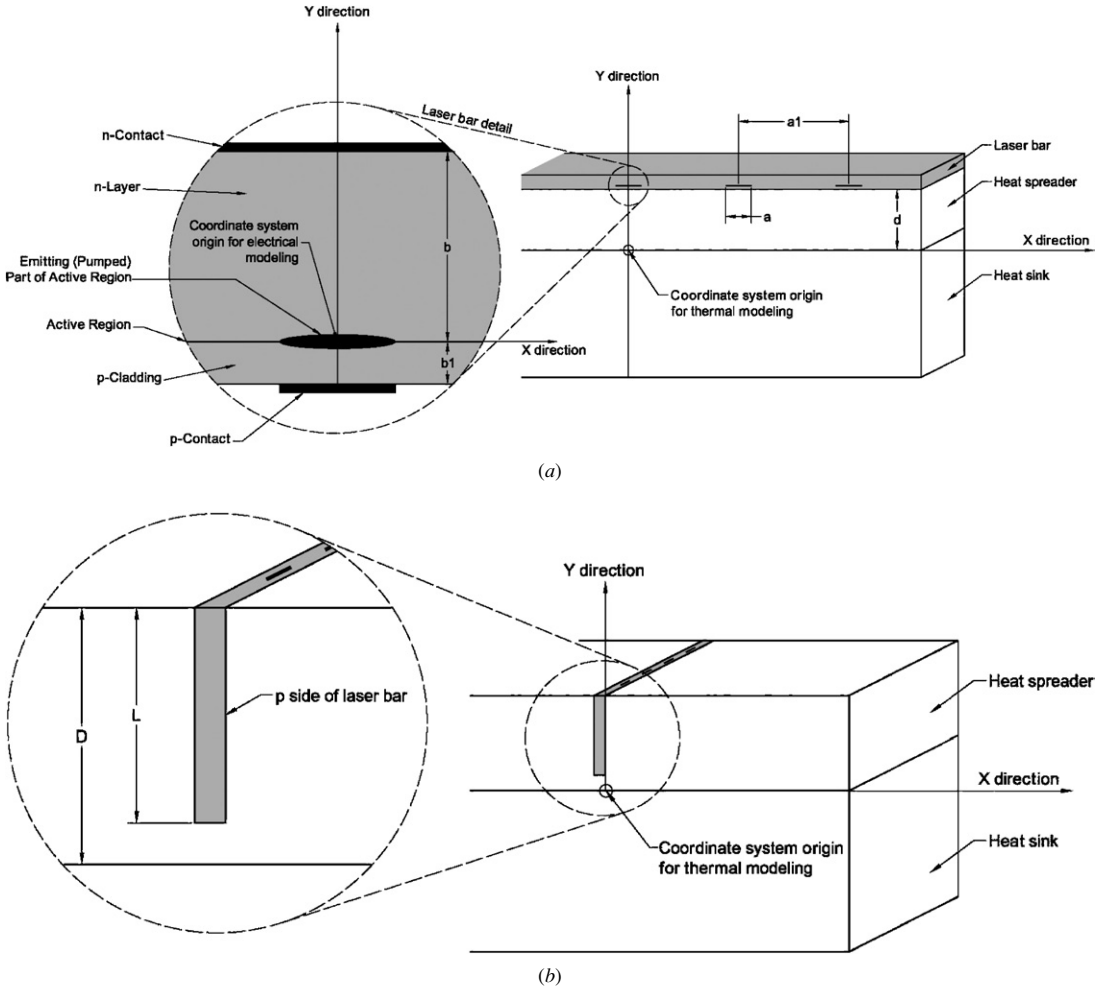

Figure 1. Perspective views of the mounted laser bar. (*a*) The planar model with the laser bar, heat spreader and heat sink describing parallel planes. Light is emitted from the electrically pumped active regions defined by the multiple p-contacts of width a. The centre-to-centre distance between p-contacts is a_1, and the thickness of the heat spreader is d. A detailed view of the laser bar is shown in the circular inset. The inset shows that the laser bar consists of an n-layer (n-cladding and substrate) of thickness b, a thin active region and a p-clad of thickness b_1. Different coordinate systems have been used. The electrical resistance modelling employs the coordinate origin shown in the inset, the thermal resistance modelling employs the coordinate origin shown in the main drawing. (*b*) The perpendicular model with a similar laser bar mounted in a grooved heat spreader. The laser bar cavity length L and heat spreader thickness D are shown in the inset. The asymmetry of the n and p layer thicknesses means that the heat transfer is through the p-side of the bar which is modelled as a planar heat source of negligible thickness.

the geometry of the laser structure and the heat spreader. The calculation of $R_T(f)$ and $r(f)$ is the main content of the paper.

Equations (2.4) and (2.5) with known $j_{th}(T)$, $\eta(T)$, $R_T(f)$ and $r(f)$ make up the basis for the optimization problems described above, and these problems can be formulated as

- Given T, find maximal P_{opt}.
- Given P_{opt}, find minimal T.

It is necessary to note that mathematically the two problems are equivalent. Given $P_{opt}(j, T, f)$ and $T(j, f)$, both of them are reduced to the solution of the equation

$$\frac{\partial P_{opt}}{\partial f}\frac{\partial T}{\partial j} - \frac{\partial P_{opt}}{\partial j}\frac{\partial T}{\partial f} = 0 \qquad (2.7)$$

together with one of equations (2.4) and (2.5). The equivalence can be seen from the results (figures 3 and 4), where the plots $P_{opt}(T)$ and $T(P_{opt})$ can be obtained from each other by the transposition of the axes.

In the next two sections, we present the calculation of $R_T(f)$ and $r(f)$ for simple but practically important models. For both cases we succeeded in obtaining analytical results that are quite flexible and convenient for practical applications.

3. Electric resistance of the bar

The model of the laser structure used for calculating the electric resistance is shown in figure 1(*a*). It consists of a p-cladding and n-layer (n-cladding with a substrate) separated by a thin region containing the waveguide and quantum wells [16]. The thickness of this quantum well region is typically smaller than 1 μm and we consider it as an interface. The n-side of the bar is uniformly covered by a metal n-contact, the p-side of the bar has multiple p-contact stripes of width a and centre-to-centre separation a_1. The thickness of the p-cladding b_1 is much smaller than the thickness of the n-layer b and the stripe width a. Previously, we considered a similar structure with one

stripe [14]. In the system with many stripes current spreads from adjacent stripes limit each other and as a result, the resistance of the structure decreases with increasing distance between the stripes. We consider a bar with a large number of stripes so that the difference of the current spread around two stripes at the edges of the bar can be neglected. Then it is possible to consider a periodical system of stripes with period a_1 and fill factor $f = a/a_1$.

Due to the small thickness of the p-cladding, the current spread in it can be neglected and the width of the pumped active region is the same as the stripe width. If the current density components in the p-cladding are $j_x = 0$, $j_y(x, y) = j_y(x, 0)$ and the potential at the contact stripe, U, is constant then the potential at the n-side of the active region is

$$U_a(x) = U - \sigma_p j_y(x, 0) - U_0, \tag{3.1}$$

where σ_p is the conductivity of the p-cladding and U_0 is the potential drop across the active region which is assumed constant above threshold.

The current spread problem for the n-layer now can be solved independently of the p-cladding. Due to high doping in the n-layer the screening radius there is very small which makes the diffusion current negligible compared to the drift current. As a result, the potential distribution in the n-layer $\phi(x, y)$ is controlled by the Laplace equation. One of the boundary conditions for this equation is a constant potential at the n-contact, $y = b$. At the pn interface the potential is $U_a(x)$ which can be considered given only in the pumped regions while between the pumped regions the current normal to the interface is zero. The solution to this problem allows one to find $j_y(x, 0)$ as a functional of $U_a(x)$. The substitution of this functional into equation (3.1) provides an equation for $U_a(x)$. The solution to this equation gives the final result. In section 3.1 the potential distribution in the n-layer is found analytically, in section 3.2 the potential $U_a(x)$ is found with the help of a variational method, and in section 3.3 the resistance of the structure is calculated.

3.1. Potential distribution in n-layer

The boundary problem for the Laplace equation in the n-layer formulated above is equivalent to the boundary problem for the complex potential,

$$\chi(z) = \phi(x, y) + \mathrm{i}\psi(x, y), \tag{3.2}$$

where $z = x + \mathrm{i}y$. Apparently, $\chi(z + a_1) = \chi(z)$ and it is enough to consider the period $|x| < a_1/2$. The system is symmetric with respect to the lines $x = \pm a_1/2$ in the middle between the stripes, and the current normal to this line is zero, $\sigma_n[\partial\phi/\partial x]_{x=\pm a_1/2} = 0$ (σ_n is the conductivity of the n-layer). Then due to Cauchy–Riemann relations,

$$\frac{\partial\phi}{\partial x} = \frac{\partial\psi}{\partial y}, \qquad \frac{\partial\psi}{\partial x} = -\frac{\partial\phi}{\partial y}, \tag{3.3}$$

the boundary conditions can be written as

$$\phi = U_a(x), \qquad -\frac{a}{2} < x < \frac{a}{2}, \qquad y = 0, \tag{3.4a}$$

$$\psi = \text{const}, \qquad \frac{a}{2} < |x| < \frac{a_1}{2}, \qquad y = 0, \tag{3.4b}$$

$$\psi = \text{const}, \qquad x = \pm\frac{a_1}{2}, \tag{3.4c}$$

$$\phi = 0, \qquad y = b. \tag{3.4d}$$

To solve this problem it is convenient to map it first to the upper half-plane of another complex variable $w = u + \mathrm{i}v$. This can be done with the help of the transformation (see, e.g., [20, 21])

$$z = CF(\arcsin w; k), \tag{3.5}$$

where $F(\theta; k)$ is the elliptic integral of the first kind. Constants C and $k < 1$ are defined by the condition that point $z = a_1/2$ is mapped onto $w = 1$ and point $z = a_1/2 + \mathrm{i}b$ is mapped onto $w = 1/k$,

$$a_1 = 2C\boldsymbol{K}(k), \tag{3.6a}$$

$$b = C\boldsymbol{K}(k'). \tag{3.6b}$$

where $\boldsymbol{K}(k) = F(\pi/2; k)$ is the complete elliptic integral of the first kind and $k' = \sqrt{1 - k^2}$. When $w \to \infty$ equation (3.5) gives $z = \mathrm{i}b$. The transformation inverse to equation (3.5) is expressed in elliptic sinus,

$$w = \mathrm{sn}(z; k). \tag{3.7}$$

Now it is necessary to find the function $\chi(w) = \phi(u, v) + \mathrm{i}\psi(u, v)$ analytic at the upper half-plane of w and satisfying the following boundary conditions at $v = 0$:

$$\phi = (U - U_0)\Phi(u), \qquad -u_a < u < u_a, \tag{3.8a}$$

$$\psi = \text{const}, \qquad u_a < |u| < 1/k, \tag{3.8b}$$

$$\phi = 0, \qquad |u| > 1/k, \tag{3.8c}$$

where

$$u_a = \mathrm{sn}(a/2C; k) < 1, \tag{3.9}$$

$$\Phi(u) = \frac{1}{U - U_0} U_a[CF(\arcsin u; k)]. \tag{3.10}$$

The solution to this problem can be found with the help of the Keldysh–Sedov method [21, 22] and is [14]

$$\chi(w) = \frac{U - U_0}{\pi}[-f(w) + \psi_0 g(w)], \tag{3.11}$$

where

$$f(w) = 2w\sqrt{(1 - k^2w^2)\left(w^2 - u_a^2\right)} \times \int_0^{u_a} \frac{\Phi(t)}{\sqrt{(1 - k^2t^2)\left(u_a^2 - t^2\right)}} \frac{\mathrm{d}t}{t^2 - w^2}, \tag{3.12a}$$

$$g(w) = 2w\sqrt{(1 - k^2w^2)\left(w^2 - u_a^2\right)} \times \int_{u_a}^{1/k} \frac{1}{\sqrt{(1 - k^2t^2)\left(t^2 - u_a^2\right)}} \frac{\mathrm{d}t}{t^2 - w^2}. \tag{3.12b}$$

Here $\sqrt{1 - k^2w^2}$ is defined on the plane of w with the cuts along the real axis from $w = 1/k$ to ∞ and from $w = -1/k$ to $-\infty$, and is positive at the real axis between the points $-1/k$ and $+1/k$. $\sqrt{w^2 - u_a^2}$ is defined on the plane of w with the cut along the real axis between the points $w = -u_a$ and $w = u_a$ and positive at the real axis at $u > u_a$. Thus, the function $\sqrt{(1 - k^2w^2)\left(w^2 - u_a^2\right)}$ is real and positive at the real

axis between the points u_a and $+1/k$ and changes sign when w changes sign. The integrals in both $f(w)$ and $g(w)$ are defined at the upper half-plane of w. They can be analytically continued to the lower half-plane across the part of the real axis where they are real.

Potential $\chi(w)$ is limited at $w \to \infty$ only if

$$\psi_0 = \frac{1}{\boldsymbol{K}\left(\sqrt{1-k^2u_a^2}\right)} \int_0^{u_a} \frac{\Phi(t)\,\mathrm{d}t}{\sqrt{(1-k^2t^2)\left(u_a^2-t^2\right)}}. \quad (3.13)$$

3.2. Potential at the active region

For the calculation of $j_y(x,0)$ it is convenient to introduce

$$j(z) = j_x(x,y) - \mathrm{i}j_y(x,y) = -\sigma_n\left(\frac{\partial\phi}{\partial x} - \mathrm{i}\frac{\partial\phi}{\partial y}\right) = -\sigma_n\frac{\mathrm{d}\chi}{\mathrm{d}z}. \quad (3.14)$$

In new variables according to equation (3.5)

$$j(w) = -\frac{\sigma_n}{C}\sqrt{(1-w^2)(1-k^2w^2)}\,\frac{\mathrm{d}\chi}{\mathrm{d}w}. \quad (3.15)$$

After the calculation of the complex potential derivative this is reduced to the form

$$j(w) = \frac{2\sigma_n(U-U_0)}{\pi C\boldsymbol{K}\left(\sqrt{1-k^2u_a^2}\right)}\sqrt{\frac{1-w^2}{w^2-u_a^2}} \times [J_1(u_a,k) - J_2(w,u_a,k)]. \quad (3.16)$$

where

$$J_1(u_a,k) = \boldsymbol{E}\left(\sqrt{1-k^2u_a^2}\right)\int_0^{\pi/2}\frac{\Phi(u_a\sin\theta)\,\mathrm{d}\theta}{\sqrt{1-k^2u_a^2\sin^2\theta}} - \boldsymbol{K}\left(\sqrt{1-k^2u_a^2}\right)k^2u_a^2\int_0^{\pi/2}\frac{\Phi(u_a\sin\theta)\sin^2\theta\,\mathrm{d}\theta}{\sqrt{1-k^2u_a^2\sin^2\theta}}. \quad (3.17a)$$

$$J_2(w,u_a,k) = \boldsymbol{K}\left(\sqrt{1-k^2u_a^2}\right)\int_0^{u_a}\Phi'(t)t \times\frac{\sqrt{(1-k^2t^2)\left(u_a^2-t^2\right)}}{t^2-w^2}\,\mathrm{d}t, \quad (3.17b)$$

and $\boldsymbol{E}(k)$ is the complete elliptic integral of the second kind.

The substitution of $j_y(u,0)$ from equation (3.16) into equation (3.1) leads to the equation

$$\Phi(u) = 1 - \frac{b_1\sigma_n}{b\sigma_p}\frac{2\boldsymbol{K}(k')}{\pi}\sqrt{\frac{1-u^2}{u_a^2-u^2}}\,J_3(u_a,k), \quad (3.18)$$

where

$$J_3(u_a,k) = \frac{J_1(u_a,k)}{\boldsymbol{K}\left(\sqrt{1-k^2u_a^2}\right)} - \mathrm{V.p.}\int_0^{u_a}\Phi'(t)t \times\frac{\sqrt{(1-k^2t^2)\left(u_a^2-t^2\right)}}{t^2-u^2}\,\mathrm{d}t. \quad (3.19)$$

Integral equation (3.18) determines $\Phi(u)$. The solution to equation (3.18) gives a minimum to the functional

$$F[\Phi] = \int_0^{u_a}\left[1-\Phi(u) - \frac{b_1\sigma_n}{b\sigma_p}\frac{2\boldsymbol{K}(k')}{\pi}\sqrt{\frac{1-u^2}{u_a^2-u^2}}\,J_3(u_a,k)\right]^2\mathrm{d}u. \quad (3.20)$$

This functional can be used to find an approximate solution with the help of the variational method. A good approximation is $\Phi(u) = c_1 - c_2u^2 - c_3u^8$.

3.3. Calculation of the resistance

The current across the n-layer is

$$I = L\int_{-a/2}^{a/2} j_y(x,0)\,\mathrm{d}x = 2L\sigma_n\psi(a/2,0) = 2L\sigma_n\psi(u_a,0), \quad (3.21)$$

where L is the length of the stripe. With the help of equation (3.11) it is possible to show that

$$\chi(u_a) = (U-U_0)[\Phi(u_a) + \mathrm{i}\psi_0], \quad (3.22)$$

and then

$$I = \frac{U-U_0}{r}, \qquad r = \frac{1}{2L\sigma_n\psi_0}. \quad (3.23)$$

The substitution of equation (3.13) gives

$$r(f) = \frac{\boldsymbol{K}\left(\sqrt{1-k^2u_a^2}\right)}{2L\sigma_n}\left[\int_0^{u_a}\frac{\Phi(t)\,\mathrm{d}t}{\sqrt{(1-k^2t^2)\left(u_a^2-t^2\right)}}\right]^{-1}. \quad (3.24)$$

If the resistance of the p-cladding can be neglected, i.e., $b_1\sigma_n/b\sigma_p \ll 1$ then $\Phi(t) = 1$ and

$$r = \frac{\boldsymbol{K}\left(\sqrt{1-k^2u_a^2}\right)}{2L\sigma_n\boldsymbol{K}(ku_a)}. \quad (3.25)$$

4. Thermal resistance

Typically the laser bar is mounted on a heat spreader and actively cooled heat sink. The thermal resistance of the laser bar crucially depends on the geometry of the heat spreader. In this section, we calculate the thermal resistance for two different models. The first is the planar model where the bar is parallel to the heat sink and is separated by a heat spreader with given thickness d (figure 1(a)). The second model represents the bar imbedded in the heat spreader perpendicular to the interface between the spreader and the heat sink (figure 1(b)). The arrays used to verify our model were fabricated using the perpendicular geometry [19]. In both models, we assume an ideal heat sink in which temperature is maintained constant at any dissipated power.

4.1. Planar geometry

In this case the temperature field in the heat spreader is two-dimensional; there is no temperature gradient along the laser cavity (figure 1(a)). The temperature distribution can be found from the equation

$$\frac{\partial^2T}{\partial x^2} + \frac{\partial^2T}{\partial y^2} = 0, \quad (4.1)$$

with boundary conditions

$$T(x,0) = 0, \quad (4.2a)$$

$$\kappa \left.\frac{\partial T}{\partial y}\right|_{y=d} = \begin{cases} q, & na_1 - a/2 < x < na_1 + a/2, \\ 0, & (n-1)a_1 + a/2 < x < na_1 - a/2. \end{cases} \tag{4.2b}$$

Here T is the temperature excess above the heat sink temperature, d is the width of the heat spreader and κ is the thermal conductivity of the heat spreader material. The heat flux from each laser equals the power dissipated there, $q = p_\mathrm{d}/La$. For the calculation of the thermal resistance of the unit length of the bar it is convenient to express the flux as the power dissipated per unit length:

$$q = \frac{P_\mathrm{d}}{fL}. \tag{4.3}$$

Due to the periodicity of the boundary conditions the solution to equation (4.1) can be found with the help of Fourier expansion and the result is

$$T(x, y) = \frac{qa}{\kappa}\left[\frac{y}{a_1} + \frac{a_1}{\pi^2 a}\sum_{n=1}^{\infty}\frac{\sin(n\pi a/a_1)}{n^2} \times \frac{\sinh(2n\pi y/a_1)}{\cosh(2n\pi d/a_1)}\cos\frac{2n\pi x}{a_1}\right]. \tag{4.4}$$

The temperature of the bar,

$$T(x, d) = \frac{qa}{\kappa}\left[\frac{df}{a} + \frac{1}{\pi^2 f} \times \sum_{n=1}^{\infty}\frac{\sin(n\pi f)}{n^2}\tanh\frac{2n\pi df}{a}\cos\frac{2n\pi xf}{a}\right], \tag{4.5}$$

oscillates with x, i.e., along the bar. It reaches its maximum in the middle of a stripe, $x = 0$, and minimum between two stripes, $x = a_1/2$. The amplitude of the oscillations decreases with increasing fill factor and at $f = 1$ the temperature of the bar is x independent: $T(x, d)|_{f=1} = qd/\kappa$

The measured laser temperature corresponds to the temperature averaged across the laser, i.e.,

$$T_\mathrm{av} = \frac{1}{a}\int_{-a/2}^{a/2} T(x, d)\,\mathrm{d}x = \frac{qa}{\kappa}\left[\frac{df}{a} + \frac{1}{\pi^3 f^2}\sum_{n=1}^{\infty}\frac{\sin^2(n\pi f)}{n^3}\tanh\frac{2n\pi df}{a}\right]. \tag{4.6}$$

This gives the following expression for the thermal resistance of the unit length of the bar,

$$R_\mathrm{T} = \frac{T_a}{P_\mathrm{d}} = \frac{d}{\kappa L} + \frac{a}{\kappa\pi^3 f^3 L}\sum_{n=1}^{\infty}\frac{\sin^2 n\pi f}{n^3}\tanh\frac{2n\pi df}{a}. \tag{4.7}$$

The thermal resistance decreases with increasing fill factor and reaches the value of $d/\kappa L$ when $f = 1$. A decreasing thermal resistance with increasing fill factor has also been obtained using the finite element method [18].

4.2. Perpendicular geometry

In the perpendicular geometry (figure 1(*b*), the temperature depends on all three coordinates: it depends on the distance from the bar, it changes along the cavity due to the varying distance to the heat sink and it changes in the direction along the bar similarly to the planar model. The exact calculation of the three-dimensional temperature field gives quite cumbersome results. However, practically it is necessary to know the temperature close to the maximal one. For the temperature close to the maximum a very good approximation can be obtained in a relatively simple way.

For this reduction, first the temperature field in the perpendicular geometry is calculated for a fill factor of 100%. Then the effective thickness of an equivalent planar geometry heat spreader is determined such that it provides the 100% fill factor bar temperature equal to the maximal temperature in the perpendicular geometry at the same 100% fill factor. After the effective thickness is chosen the bar temperature can be calculated with any fill factor with the help of equation (4.7). An excellent matching of this approximation to experimental results has been achieved.

The calculation of the maximal temperature in the perpendicular geometry with a fill factor of 100% is reduced to a two-dimensional problem for equation (4.1) at a stripe with a cut (see figure 1(*b*)). The boundary conditions for this equation are the following. The temperature excess equals zero at the interface with the heat sink, $y = 0$. The heat flux comes in only from the p-side of the bar, $D - L < y < D, x = +0$. The heat flux from the n-side, $D - L < y < D, x = -0$, can be neglected because of the large thickness of the substrate compared to the thickness of the p-cladding. That is

$$T(x, 0) = 0, \qquad \left.\frac{\partial T}{\partial y}\right|_{y=D} = 0, \tag{4.8a}$$

$$\left.\frac{\partial T}{\partial x}\right|_{\substack{x=-0 \\ D-L<y<D}} = 0, \qquad \kappa\left.\frac{\partial T}{\partial x}\right|_{\substack{x=+0 \\ D-L<y<D}} = -q. \tag{4.8b}$$

The problem can be solved with the conformal mapping of the stripe with the cut $x = 0, D - L < y < D$ at the plane $z = x + \mathrm{i}y$ to the stripe $0 < v < \pi$ at the plane $w = u + \mathrm{i}v$. The mapping is carried out with the help of the function [21]

$$w = \ln\frac{\cos\frac{\pi L}{2D}\sqrt{\coth^2\frac{\pi z}{2D} + \tan^2\frac{\pi L}{2D}} + 1}{\cos\frac{\pi L}{2D}\sqrt{\coth^2\frac{\pi z}{2D} + \tan^2\frac{\pi L}{2D}} - 1}. \tag{4.9}$$

The Laplace equation for T in the plane z remains the Laplace equation in the plane w. The boundary conditions at the plane w are

$$T(u, 0) = 0, \tag{4.10a}$$

$$\left.\frac{\partial T}{\partial v}\right|_{v=\pi} = \begin{cases} \dfrac{q}{\kappa}\dfrac{D}{\pi}\dfrac{\cos\frac{\pi L}{2D}\tanh\frac{u}{2}}{\sqrt{\sin^2\frac{\pi L}{2D} - \tanh^2\frac{u}{2}}}, & 0 < u < u_D, \\ 0, & \text{otherwise.} \end{cases} \tag{4.10b}$$

The solution in the stripe $0 < v < \pi$ can be found with the help of expansion in Fourier integral in u or Fourier series in v and the result can be reduced to the form

$$T(u, v) = \frac{1}{2\pi}\frac{qD}{\pi\kappa}\int_0^{u_D}\ln\left[\frac{\cosh[(u-u')/2] + \sin(v/2)}{\cosh[(u-u')/2] - \sin(v/2)}\right] \times \frac{\cos\frac{\pi L}{2D}\tanh\frac{u'}{2}}{\sqrt{\sin^2\frac{\pi L}{2D} - \tanh^2\frac{u'}{2}}}\,\mathrm{d}u'. \tag{4.11}$$

The temperature reaches its maximum at $y = D, x = +0$ or $u = u_D, v = \pi$ and it is

$$T_m = \frac{1}{2\pi}\frac{qD}{\pi\kappa}\int_0^{u_D} \ln\left[\frac{\cosh[(u_D-u)/2]+1}{\cosh[(u_D-u)/2]-1}\right] \times \frac{\cos\frac{\pi L}{2D}\tanh\frac{u}{2}}{\sqrt{\sin^2\frac{\pi L}{2D}-\tanh^2\frac{u}{2}}}\,\mathrm{d}u. \quad (4.12)$$

A comparison of this expression with the temperature in the plane geometry for $f = 100\%, T_m = qd/\kappa$, immediately gives the following expression for the effective thickness:

$$d = \frac{D}{2\pi^2}\int_0^{u_D} \ln\left[\frac{\cosh[(u_D-u)/2]+1}{\cosh[(u_D-u)/2]-1}\right] \times \frac{\cos\frac{\pi L}{2D}\tanh\frac{u}{2}}{\sqrt{\sin^2\frac{\pi L}{2D}-\tanh^2\frac{u}{2}}}\,\mathrm{d}u. \quad (4.13)$$

Now the thermal resistance can be calculated with the help of equation (4.7) where d is taken from equation (4.13).

5. Results and discussion

We compare our optimization theory with results obtained on laser bars based on InGaAsP/InP and operating at 1.5 μm. The measurements were made on bars with different fill factors, 10%, 20% and 40%. In all bars the width of the n-contact stripes was $a = 100$ μm. The distance between the n- and p-contacts was 140 μm, the thickness of the p-cladding was $b_1 = 1.5$ μm and the conductivities of the n-layer and p-cladding were $\sigma_n = 320$ Ω^{-1} cm^{-1} and $\sigma_p = 1.6$ Ω^{-1} cm^{-1}. This gives the ratio of the resistances of the p-cladding and the n-layer necessary for the calculation of the electric resistance $b_1\sigma_n/b\sigma_p = 2$ (here b_1 and σ_p are the thickness of the conductivity of the p-cladding).

The laser bars were mounted in metallized grooves in BeO heat spreaders which were bonded to water-cooled microchannel heat sinks (figure 1(*b*)). The thickness of the heat spreader was $D = 1.5$ mm, and the cavity length for these bars was 1 mm. According to section 4.2 the thermal resistance of the bar in this geometry is equivalent to the thermal resistance in the planar geometry (figure 1(*a*)), with an effective thickness of $d = 8.3a$ obtained from equation (4.13). Using $d = 830$ μm in equation (4.7) the thermal resistance was calculated for laser bars in the perpendicular geometry for different bar designs. These results were compared to experimentally measured thermal resistances. The measured dependence of the active region overheating versus the dissipated power density is given in figure 2(*a*). The slopes of the straight lines fitted to the experimental data in figure 2 provide estimates of the thermal resistance for bars with different fill factors. Thermal resistances of bars with f equal to 0.1, 0.2 and 0.4 are, respectively, 0.56, 0.40 and 0.36 K cm W^{-1}. The standard deviation of measured points from the linear fits gives the accuracy of the thermal resistance around 4% or smaller. The maximal error coming from the error of the temperature measurements is close to this value. Equation (4.7) gives for these bars 0.58, 0.41 and 0.35 K cm W^{-1}. That is the discrepancy between the theoretical and experimental results is within the accuracy of the measurements. The thermal resistances of bars with

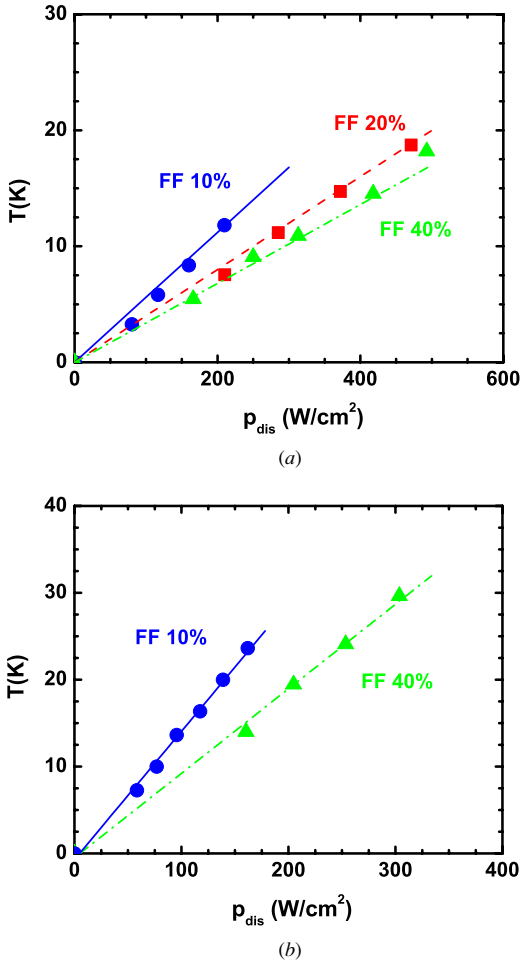

Figure 2. Measured overheating of the active region versus dissipated power density p_{dis} (*a*) for different fill factor laser bars with 1 mm long cavities mounted in BeO heat spreaders and (*b*) for different fill factor laser bars with 2 mm long cavities mounted in CuW heat spreaders. Solid symbols indicate data points (circles, squares, and triangles for 10%, 20%, and 40% fill factors respectively). Lines fit to the experimental data are used to determine the thermal resistance.

2 mm cavities mounted in heat spreaders of CuW were also evaluated (figure 2(*b*)). For these bars, we compare the ratio of the thermal resistances for the 0.1 and 0.4 fill factor bars. The experimentally determined ratio is 1.5, close to the calculated ratio of 1.64.

Along with the calculated dependences of $r(f)$ and $R_T(f)$, the temperature dependences of the threshold current and slope efficiency are required to solve the optimization problem (2.7). These parameters were measured under short pulse operation by changing the heat sink temperature for individual 1 mm cavity length lasers. Both the threshold current j_{th} and slope efficiency η are well described by equation (2.6) with $j_{\mathrm{r}} = 0.5$ A, $\eta_{\mathrm{r}} = 0.5$ W A^{-1}, $T_{\mathrm{r}} = 20$ C, $T_0 = 54$ K and $T_1 = 160$ K. The voltage across the active region above threshold $U_0 = 0.91$ V.

The solution of the optimization problem (equation (2.7)) yields the maximum output power for a given active region temperature rise, as shown by the solid line in figure 3. The dashed line in figure 3 corresponds to the optimal fill factor design that provides this output power at the given active region

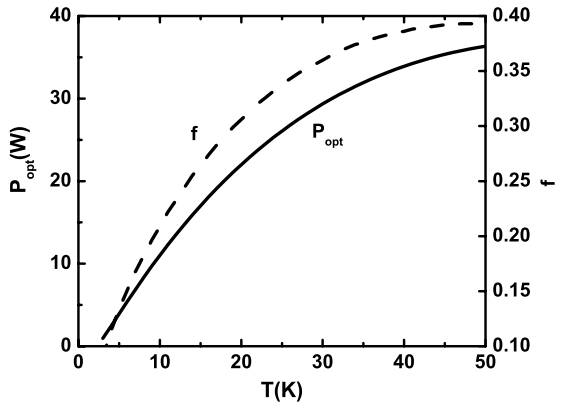

Figure 3. Optimized fill factor (dashed line) and corresponding maximum output power (solid line) as a function of laser temperature rise.

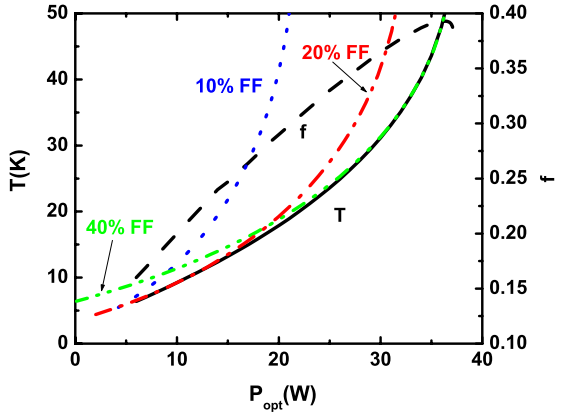

Figure 4. Optimized fill factor (dashed line) and corresponding minimal laser temperature rise (solid line) as a function of output power. The dotted lines show the temperature rise for several fixed fill factor arrays as a function of output power.

temperature rise. A similar optimization based on minimal temperature rise for a given output power is shown in figure 4. Here again, the dashed line represents the optimal fill factor, and the solid line indicates the minimal active region temperature rise for the given output power.

To understand how critical the optimal fill factor is, we compare the analytically calculated active region temperature rise versus output power for an optimal fill factor array and for several fixed (10%, 20% and 40%) fill factor arrays. This comparison is given in figure 4. The 40% fill factor array plot is nearly coincident with the optimal fill factor plot above about 25 W. For output powers below 17 W, the difference in active region temperature between the optimal array and the 20% fill factor array is negligible. The 10% fill factor array has the highest temperature among the rest arrays above 5 W. Clearly, the optimal fill factor depends on the bar operating regime.

Earlier we suggested two methods of increasing array output power: increasing the pumping current per emitter and increasing the number of emitters. By calculating the optimal fill factor for a particular operating regime, we have found the most favourable balance between these two approaches. The optimal fill factor curve shown in figure 3 illustrates that for increasing output power in this system, it is preferable to use a higher fill factor. Higher fill factors offer advantages for higher power operation since the effect of mutual heating is weaker than the heating of each one of them by the current.

6. Conclusion

In this paper

- We obtained analytical expressions for the steady state electrical and thermal resistance of a laser bar. Both quantities depend on geometry, and in particular, the fill factor.
- Theoretical results for the thermal resistance are in excellent agreement with the measured thermal resistance of 1 and 2 mm cavity length laser arrays with different fill factors.
- We use the analytical results to calculate the optimal laser bar fill factor. The value of the optimal fill factor depends on the working regime of the bar; higher output powers require higher fill factors for minimum active region temperatures.

Acknowledgments

This material is based upon work supported by the United States Air Force under contract nos. FA9550-04-C-0021 and FA9550-05-C-0043.

References

[1] Erbert G, Bärwolff A, Sebastian J and Tomm J 2000 High-power broad-area diode lasers and laser bars *High-Power Diode Lasers (Lasers, Topics Appl. Phys.* vol 78*)* ed R Diehl (Berlin: Springer) p 173
[2] Maiorov M, Menna R, Khalfin V, Milgazo H, Matarese R, Garbuzov D and Connolly J 1999 *IEEE Photon. Technol. Lett.* **11** 961
Maiorov M, Menna R, Khalfin V, Milgazo H, Triano A, Garbuzov D and Connolly J 1999 *Electron. Lett.* **35** 636
[3] Botez D and Scifres D R (ed) 1994 *Diode Laser Arrays* (Cambridge: Cambridge University Press)
[4] Joyce W B and Wemple S W 1970 *J. Appl. Phys.* **41** 3818
Joyce W B and Dixon R W 1975 *J. Appl. Phys.* **46** 856
[5] Yonezu H, Sakuma I, Kobayashi K, Kamejima T, Ueno M and Nannichi Y 1973 *Japan. J. Appl. Phys.* **12** 1585
[6] Dumke W P 1973 *Solid-State Electron.* **16** 1279
[7] Buus J 1979 *IEEE J. Quantum Electron.* **15** 734
[8] Streifer W, Burnham R D and Scifres D R 1982 *IEEE J. Quantum Electron.* **18** 856
[9] Lengyel G, Meissner P, Patzak E and Zschauer K-H 1982 *IEEE J. Quantum Electron.* **18** 618
[10] Wilt D P and Yariv A 1981 *IEEE J. Quantum Electron.* **17** 1941
[11] Joyce W B 1980 *J. Appl. Phys.* **51** 2394
[12] Agrawal G P 1984 *J. Appl. Phys.* **56** 3100–9
[13] Papannareddy R, Ferguson W E Jr and Butler J K 1988 *IEEE J. Quant. Electron.* **24** 60
[14] Laikhtman B, Gourevitch A, Donetsky D, Westerfeld D and Belenky G 2004 *J. Appl. Phys.* **95** 3880
[15] Joyce W B and Dixon R W 1974 *J. Appl. Phys.* **46** 855
[16] Gourevitch A, Laikhtman B, Westerfeld D, Donetsky D, Belenky G, Trussell C W, Shellenbarger Z, An H and Martinelli R U 2005 *J. Appl. Phys.* **97** 084503–1
[17] Sarzala R P and Nakwaski W 1990 *J. Therm. Anal.* **36** 1171
Sarzala R P and Nakwaski W 1993 *J. Therm. Anal.* **39** 1297
[18] Bärwolff A, Puchert R, Enders P, Menzel U and Ackermann D 1995 *J. Therm. Anal.* **45** 417

[19] Gourevitch A, Belenky G, Donetsky D, Laikhtman B, Westerfeld D, Trussell C W, An H, Shellenbarger Z and Martinelli R 2003 *Appl. Phys. Lett.* **83** 617
[20] Nehari Z 1952 *Conformal Mapping* (New York: Dover)
[21] Lavrentev A and Shabat B V 1958 *Metody teorii funktsii kompleksnogo peremennogo* (Moskva: Gos. izd-vo fiziko-matematicheskoi lit-ry)
Lawrentjew M A and Schabat B W 1967 *Methoden der komplexen Funktionentheorie. (Mathematik fr Naturwissenschaft und Technik* Bd 13*)* bersetzung: Udo Pirl, Reiner Khnau [und] Lothar v. Wolfersdorf. (Berlin: Deutscher Verlag der Wissenschaften) (German edn)
[22] Gakhov F D 1966 *Boundary Value Problems* (New York: Dover)